Assessment of the Webb-Pearman-Leuning Correction Method for Estimating CO_2 Flux in a Tropical Coastal Sea

Muhammad Fikri Sigid[1], Yusri Yusup[1,2], Abdulghani Essayah Swesi[1], Haitem M Almdhun[1], and Ehsan Jolous Jamshidi[1]

5 [1]Environmental Technology, School of Industrial Technology, Universiti Sains Malaysia, USM 11800, Pulau Pinang, Malaysia
[2]Centre for Marine & Coastal Studies (CEMACS), Universiti Sains Malaysia, Pulau Pinang, Malaysia

Correspondence to: Yusri Yusup (yusriy@usm.my)

Abstract. CO_2 fluxes in coastal waters are vital for the global carbon cycle. The Eddy Covariance technique was used with

10 open-path gas analyzers to estimate CO_2 fluxes. However, these analyzers can lead to overestimation due to water vapor and temperature effects, and the Webb-Pearman-Leuning (WPL) correction method was applied to improve the accuracy of the estimated CO_2 flux. This study investigates the application of the WPL correction method on CO_2 flux measurements over a tropical coastal sea location. The analysis reveals that the CO_2 flux in the coastal waters mainly functions as a sink, with the diel cycle showing smaller flux magnitudes during the day and increased uptake during the night. The application of the

15 WPL correction can result in sign changes of CO_2 flux, indicating a shift from a CO_2 sink to a CO_2 source. These sign changes occur frequently, particularly during afternoon hours, and can significantly impact the implications regarding carbon exchange. The WPL correction parameters, especially those related to temperature and water vapor fluctuations, play crucial roles in influencing the CO_2 flux variations. The decrease in dry air molar density and increased vertical wind speed within the correction related to water vapor fluctuations are the major reasons for the sign change of the CO_2 flux. Based on the

20 quality flagging of the WPL correction, the non-sign change CO_2 fluxes are predominantly considered reliable data, while most of the sign change fluxes should be specially checked.

1 Introduction

Carbon dioxide (CO_2) fluxes can be directly estimated using the eddy covariance (EC) technique (Burba et al., 2013). The EC method is often used by ecosystem researchers because it has the advantage of quantifying mass (e.g., CO_2, methane,

25 water, etc.) and energy (sensible and latent heat) exchanges of expansive areas, such as forests, croplands, and oceans (Tokoro and Kuwae, 2018; Heimsch et al., 2021; Lokupitiya et al., 2016; Nakai et al., 2008; Chien et al., 2018).

The EC method uses the understanding of the behavior of turbulent eddies and utilizes vertical turbulent exchange principles to calculate the flux using the covariance of the high-frequency mixing ratio of CO_2 or moisture and the vertical velocity

30 component of the wind (McGowan et al., 2016; Stull, 1988). High-frequency measurements of wind velocity components are

afforded by sonic anemometers, but the measurement of CO_2 or moisture (H_2O) mixing ratio requires fast-response analyzers. The Infrared Gas Analyzers (IRGA) can be utilized to measure CO_2 or H_2O mixing ratios at high frequencies (e.g., 10 or 20 Hz). At high frequencies, the rapid-response analyzer could capture turbulent exchange and be able to satisfy the EC method requirement (Jones and Smith, 1977).

35

In air-sea CO_2 flux measurements, Webb et al. (1980) introduced a correction method of the Webb-Pearman-Leuning (WPL), which accounts for air density influenced by water vapor and latent heat to address the overestimation error in CO_2 flux measured by open-path gas analyzers, caused by the effects of water vapor and temperature (Edson et al., 2011; Broecker et al., 1986; Else et al., 2011). The WPL formulation was developed to eliminate the effects of air density fluctuations on the molar density of CO_2 that could occur in open-path systems (Burba et al., 2008; Miller et al., 2010). Variables of temperature, pressure, and molar density are calculated by the formula to produce the corrected CO_2 flux from the gas analyzer. The correction is also necessary because fluctuations in temperature and humidity cause fluctuations in trace gas concentrations and can simulate CO_2 flux (Jentzsch et al., 2021), and positive or negative vertical wind velocities can correspond to positive or negative corrections in flux (Liebethal and Foken, 2003). Moreover, Massman and Tuovinen (2006) confirmed the validity of formulating the WPL terms in terms of the dry air density fluctuations that interpret correctly the turbulent exchange flux, signifying the importance of the WPL correction as an approach to accurate and reliable measurements of surface exchange fluxes.

The significance of the WPL correction factor depends on the ratio between the turbulent fluctuation in constituent concentration and its mean concentration. A smaller ratio in this regard highlights the greater importance of the WPL correction (Webb et al., 1980). According to Liebethal and Foken (2003), the application of the WPL correction for CO_2 flux is considered very important among the constituent fluxes. Their research further demonstrated that the correction has a substantial impact on CO_2 flux values, leading to changes of 20% to 30%, significantly higher than the effect on latent heat flux, which only amounts to 2% to 3% of the flux.

55

Nevertheless, the WPL correction could potentially introduce inaccuracies in water vapor and carbon dioxide measurements with an open-path gas analyzer (Jentzsch et al., 2021). The correction applied to the observed flux can be large, which might potentially lead to significant changes in the measured CO_2 flux (Mauder et al., 2021). Moreover, applying the WPL correction can significantly alter CO_2 fluxes and lead to unrealistic outcomes in flux measurements under certain circumstances and conditions, especially in relevant cases with small CO_2 fluxes on the order of 1 μmol m^{-2} s^{-1} (Jentzsch et al., 2021).

Some researchers reported that the coastal region is a weak carbon source or uptake (Borges et al., 2005). The net CO_2 flux measured in northwestern Taiwan was -1.75 ± 0.98 μmol m^{-2} s^{-1}, with the diurnal flux influenced by local wind speed.

65 Similarly, in Todos Santos Bay, Mexico, the CO_2 flux was -1.32 ± 8.94 µmol m^{-2} s^{-1} (Gutiérrez-Loza and Ocampo-Torres, 2016). The CO_2 flux at Bodega Bay, California, was also a weak source, with 0.39 ± 1.84 µmol m^{-2} s^{-1} during the upwelling period and 0.05 ± 0.79 µmol m^{-2} s^{-1} during the relaxation period (Ikawa et al., 2013). Despite their importance, there is still notable uncertainty in how to parameterize these fluxes for global climate models, and more observations are necessary to gain a better understanding of the role of coastal seas in the global carbon cycle (Chien et al., 2018; Doney et al., 2009;

70 Gutiérrez-Loza and Ocampo-Torres, 2016). Additionally, measuring these fluxes using techniques and corrections is challenging because of the high uncertainties introduced during data processing, especially for smaller fluxes (Else et al., 2011; Prytherch et al., 2010). Coastal waters can display high variability in CO_2 flux due to various factors, such as water temperature, salinity, and biological activity (Ikawa et al., 2013). Despite this, wind speed plays a critical role in controlling the magnitude of air-sea CO_2 exchanges, and low wind speeds can restrict gas transfer, resulting in reduced CO_2 fluxes in

75 some cases (Aalto et al., 2021). The flux over the coast is low compared to fluxes on land (Zhang et al., 2014; He et al., 2015), and low wind speed over the coast can be one of the reasons that limit gas transfer modulation over coastal waters (Gutiérrez-Loza and Ocampo-Torres, 2016).

Accurate measurements of CO_2 flux in coastal waters are essential for a comprehensive understanding of global carbon

80 processes and for ensuring the precision of future carbon source and sequestration projection studies. Moreover, minor errors could have a significant impact on cumulative fluxes, emphasising a cautious and meticulous approach in interpreting these fluxes (Jentzsch et al., 2021). Given that the WPL correction method has been reported to potentially introduce inaccuracies in CO_2 flux measurements, especially in cases of small fluxes, it raises a question regarding its application to CO_2 flux measurements in coastal waters. Therefore, the objective of this paper is to assess the WPL correction method in measuring

85 CO_2 flux at a tropical coastal water location.
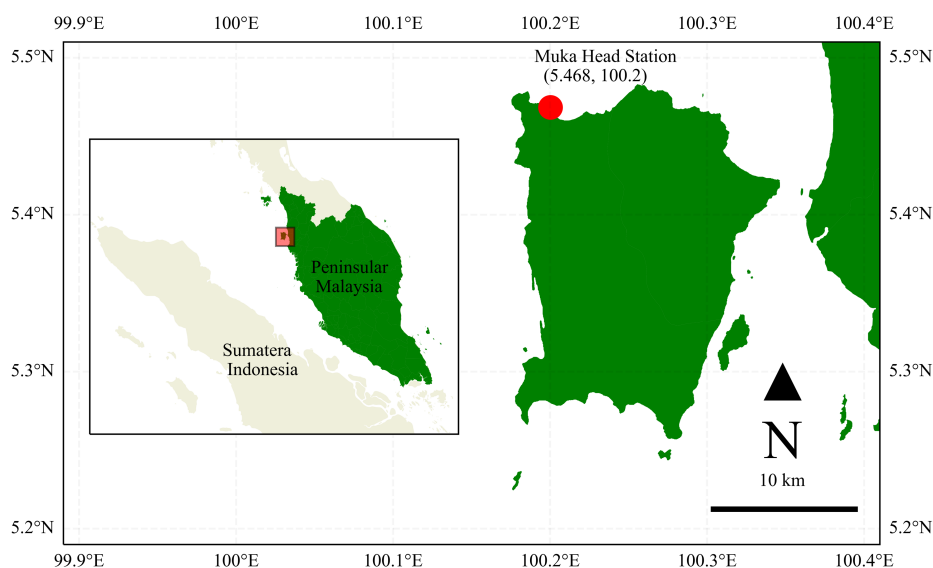

2 Materials and Methods

2.1 The EC Dataset

This analysis uses the *in-situ* EC data collected from an automated weather station called the "Muka Head Station" in the Centre for Marine and Coastal Studies of Universiti Sains Malaysia. The station is located on the northwestern part of

90 Penang, Peninsular Malaysia, at 5°28′06"N, 100°12′01"E, as shown in Fig. 1.

The station measures CO_2 and H_2O fluxes and bio-meteorological parameters (global radiation, net radiation, seawater temperature, etc.) of a tropical coastal ocean in the Strait of Malacca. The flux is calculated from the 20-Hz data collected by the open-path LI-7500 infrared CO_2/H_2O analyzer (LI-COR, USA) and a sonic anemometer (RM81000, Young, USA)

95 (Yusup et al., 2018a). The water level at this spot measures 1.5 meters, and the surface below is composed of sand. The

research site is located on a continental shelf that directly links to the Straits of Malacca, and the site is exposed to minimal anthropogenic influence (Yusup et al., 2018; Yusup et al., 2020).

Figure 1: Red circle and box show the location of the automated weather station called the Muka Head Station in Penang, Peninsular Malaysia.

From the entire list of variables available in the dataset, the primary variable analyzed was the EC's CO_2 flux. The data is accessible at http://atmosfera.usm.my and has a time resolution of 30 minutes. The dataset spanned from 2015 to 2023, but for this analysis, the temporal scope was limited to January 2016 to December 2016 due to the availability of more complete data during the period.

In this research, CO_2 fluxes associated with winds originating from directions >315° and <45° were retained, whereas the fluxes with winds coming from other directions were removed during the data processing. This was based on the standard deviation ratio for the vertical wind speed component and the friction velocity, applicable only to wind directions >315° and <90° (Yusup et al., 2018b). Furthermore, wind speed data collected inland from the south to the west of the station (>45° and <315°) were omitted because of the poor-quality flags in the recorded measurements. CO_2 flux measurements obtained during rainfall were excluded because of the effects of precipitation on the accuracy of the eddy covariance instruments.

4

2.2 Calculations of the Raw and WPL-Corrected CO_2 Fluxes

This study utilized conventional flux calculations that typically rely on density measurements obtained from gas analyzers based on light absorption (Burba et al., 2012). Afterward, density corrections, as described by Webb et al. (1980) and hereafter referred to as WPL, were applied:

$$F_c = \overline{w'\rho_c'} + (1 + \mu\sigma)\frac{\overline{\rho_c}}{\overline{T}}\overline{w'T'} + \mu\frac{\overline{\rho_c}}{\overline{\rho_a}}\overline{w'\rho_v'} + (1 + \mu\sigma)\frac{\overline{\rho_c}}{\overline{P}}\overline{w'P'} \qquad (1)$$

where F_c is WPL-corrected CO_2 flux, ρ_c is molar density of CO_2 and w is vertical component of wind speed, T is temperature, P is pressure, ρ_c is molar density of CO_2, ρ_v is molar density of water vapor, ρ_a is molar density of dry air (Webb et al., 1980). Meanwhile, $\sigma = \rho_v/\rho_a$ and $\mu = M_a/M_v$ with M_a is molecular weight of dry air, M_v is molecular weight of water vapor. Overbars represent temporal averages, while primes indicate turbulent deviations from these averages.

The first term on the right-hand side of Eq. (1) is the raw flux covariance, applying the vertical turbulence exchange concept to calculate the flux by using the vertical wind velocity and molar density of CO_2. The first term on the equation also refers as the raw CO_2 flux ($F_{c,0}$), namely the CO_2 flux that has not been corrected by WPL. Moreover, the WPL formula consists of the corrections for temperature, water vapor, and pressure fluctuations in the open-path gas analyzer, which are stated in the second, third, and fourth terms in Eq. (1). The WPL-corrected CO_2 flux (F_c) is then analysed and compared to the raw CO_2 flux ($F_{c,0}$).

2.3 Quality Flagging of the WPL Correction

The quality flagging of the WPL correction (QF$_{WPL}$) was implemented for the quality identification of WPL-corrected CO_2 flux, specifically as an approach to mark measurement with immense values of WPL correction, as standard error analyses of eddy-covariance data do not consider the unique nature of potential errors in WPL correction (Jentzsch et al., 2021; Mauder et al., 2013). The QF$_{WPL}$ parameter represents the ratio of the WPL correction to the corrected CO_2 flux, calculated using Eq. (2) below:

$$QF_{WPL} = \frac{\mu\frac{\overline{\rho_c}}{\overline{\rho_a}}\overline{w'\rho_v'} + (1 + \mu\,\sigma)\overline{\rho_c}\frac{\overline{w'T'}}{\overline{T}}}{\overline{w'\rho_c'} + \mu\frac{\overline{\rho_c}}{\overline{\rho_a}}\overline{w'\rho_v'} + (1 + \mu\,\sigma)\overline{\rho_c}\frac{\overline{w'T'}}{\overline{T}}} \qquad (2)$$

In accordance with general quality flag systems (Foken and Wichura, 1996; Foken et al., 2012), |QF$_{WPL}$| ≤ 0.5 is categorized as very good, 0.5 < |QF$_{WPL}$| ≤ 1 is classified as good, and any values exceeding |QF$_{WPL}$| > 1 requires a thorough check.

3 Results and Discussion

3.1 The CO₂ Flux Hourly Cycle at the Tropical Coast

Throughout the sampling time domain, CO_2 flux at the study location acted as CO_2 uptake, with the average values of $F_{c,0}$ and F_c are –0.14 and –0.0061 μmol m^{-2} s^{-1}, respectively. In the diel cycle in Fig. 2, the lowest CO_2 flux occurred during the daytime, with the flux closing to equilibrium. The lower flux magnitudes can be attributed to the decrease in wind speed during this period, which lowers the transfer velocity and reduces CO_2 flux in accordance with the bulk formula (Wanninkhof, 1992; Wanninkhof et al., 2009). Furthermore, the CO_2 flux varied with the hours changing between positive and negative flux, in which CO_2 flux during the nighttime displayed greater uptake movements reaching around –0.4 μmol m^{-2} s^{-1} until morning when the flux started tending to be CO_2 source to over 0.2 μmol m^{-2} s^{-1}.

The CO_2 flux during this study is similar to the CO_2 flux reported in the Rey–Sánchez et al. (2017) study as carbon uptake, which was conducted at the coastal waters of the Gulf of Aqaba, Israel. Of note is the flux magnitude of this site is substantially lower than the cited study's flux (–1.05 μmol m^{-2} s^{-1}). and F_c. Notably, it displays pronounced increases and decreases in CO_2 fluxes, including instances where the coastal region acts as a source of CO_2 during specific periods. Nevertheless, disparities in the temporal patterns are still noticeable. In the reported study, the coast demonstrates CO_2 emission (positive fluxes) around 18:00 LT, with negative fluxes starting to decrease from 06:00 LT. In contrast, the fluxes in this study illustrate the coast acting as a CO_2 source during the day, with the negative fluxes beginning to decline in the early morning hours.

The standard errors of the mean for the CO_2 fluxes are in a range of 0.01 μmol m^{-2} s^{-1} to 0.3 μmol m^{-2} s^{-1}. A notable level of uncertainty is found during the morning and evening, but a lower level is observed from 10:00 LT until 19:00 LT when the CO_2 flux exhibits less deviation, although sign-changing is more frequent during this period. The observed high uncertainty during specific times may be attributed to fluctuations in evaporation. For instance, an increase in the uncertainty around 08:00 LT was observed due to quite intense fluctuations in vertical wind speed, which may have influenced the CO_2 flux's uncertainty.

As shown in Fig. 2c, the sensible heat flux is positive, ranging from 0.5 to 2.5 W m^{-2}, with an average of 1.35 W m^{-2}. The peak occurred around 08:00 LT and 09:00 LT, during which the positive sensible heat flux exceeded 2 W m^{-2}. The magnitude of sensible heat flux can influence the WPL correction absolute value (Jentzsch et al., 2021). Positive (negative) CO_2 flux with positive (negative) sensible heat flux would increase CO_2 emission (uptake). Meanwhile, in instances of carbon uptake with positive sensible heat flux, the CO_2 flux would decrease, and the same holds for emissions in the presence of negative sensible heat fluxes.
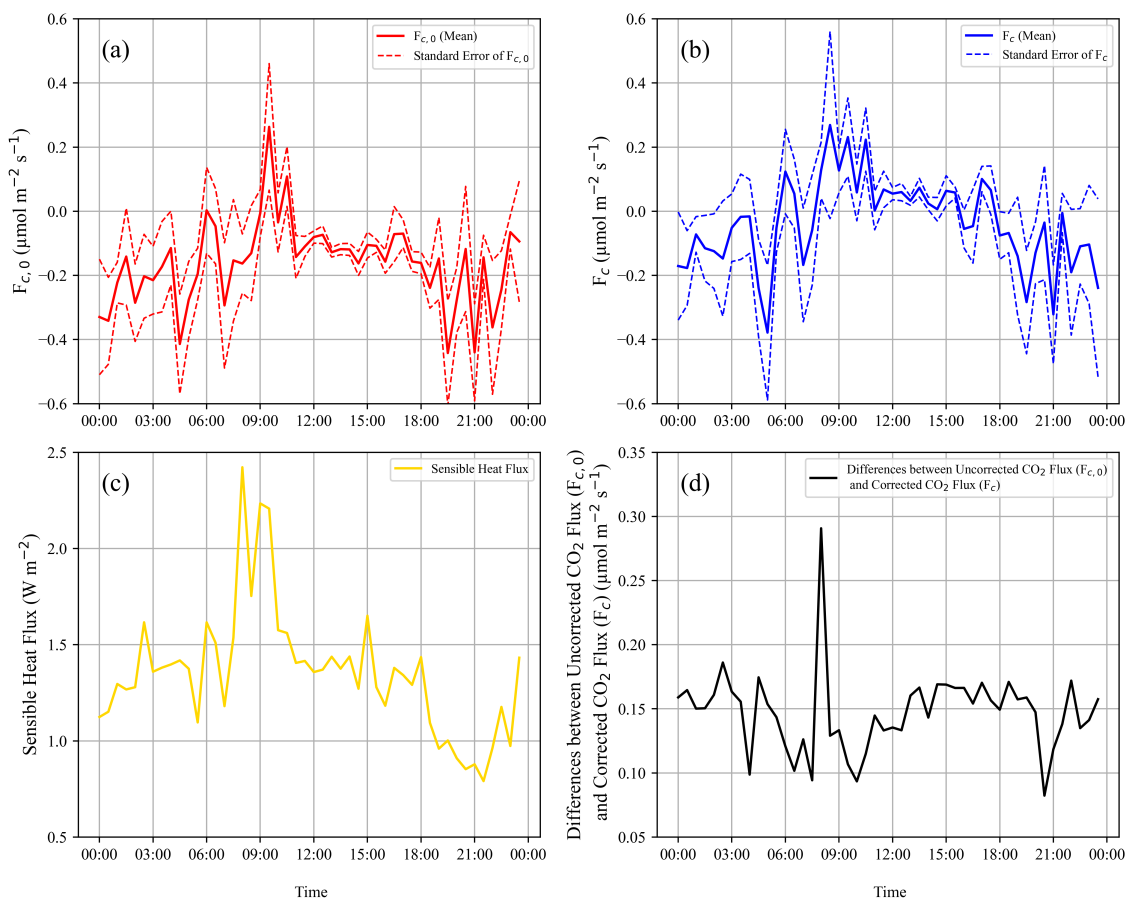
Figure 2: The climatological variation of diel (a) $F_{c,0}$, (b) F_c, (c) sensible heat flux, and (d) difference value between
180   **$F_{c,0}$ and F_c in 2016.**

The difference between F_c and $F_{c,0}$, shown in Fig. 2d, is generally within the range of 0.05–0.2 µmol m^{-2} s^{-1}. Distinctively, the difference value at 08:00 LT is 0.29 µmol m^{-2} s^{-1}, with a substantial increase of 0.2 µmol m^{-2} s^{-1} from the prior time (07:30 LT) and a noticeable decrease of 0.16 µmol m^{-2} s^{-1} at the following time (08:30 LT). The WPL correction,
185   particularly the third term, could have contributed to the high difference value at 08:00 LT.

The result in difference value between F_c and $F_{c,0}$ is similar to the observation on the open sea by (Kondo and Tsukamoto, 2007), albeit the magnitude difference in this research is not as significant. The magnitude difference by the WPL correction in the cited study is higher by 1.40 µmol m^{-2} s^{-1}. The large difference in the latter study was accompanied by a higher
190   average magnitude of the $F_{c,0}$ reaching up to 1.42 µmol m^{-2} s^{-1}, which can be due to the location of their study, i.e., the open sea with strong winds. Nevertheless, F_c is much lower than $F_{c,0}$ by over 90% for both over the sea and the coastal waters, and

it results in a CO_2 flux value being close to the CO_2 flux calculated using the bulk transfer equation as measured in (Kondo and Tsukamoto, 2007).

195   In addition, the diel cycle between $F_{c,0}$ and F_c shows that F_c has more positive fluxes during the daytime as well as lower negative fluxes due to the WPL correction. In this case, the WPL correction can cause the negative fluxes of the $F_{c,0}$ to change to positive fluxes shown by the F_c, which indicates the change in the role of the coast as a sink of CO_2 into a CO_2 source. The $F_{c,0}$ has the positive fluxes between 09:00 LT and 11:00 LT, whereas the F_c tends to have the positive flux during 05:00 LT until 18:00 LT. Based on research by Jentzsch et al. (2021), the WPL correction applied to CO_2 fluxes

200   smaller than 5 µmol m^{-2} s^{-1} can result in correction values higher than the actual fluxes, which may lead to an uncertain interpretation. Consequently, the different results, particularly in the change of the negative sign to the positive sign of the CO_2 flux, can drastically change the conclusion of the carbon exchange in the studied location.

3.2 Sign Change and Non-Sign Change Occurrences

During the study period, there were 2689 30-minute data points in 2016. By separating the data into sign change and non-

205   sign change categories, there were 1237 occurrences of non-sign change, accounting for approximately 46% of the available data. Meanwhile, there were 1452 sign change events, representing around 54% of the available data, slightly higher than the non-sign change occurrences and indicating a significant number of sign change events.

Based on the graph in Fig. 3, sign changes occurred in each 30-minute interval. However, the number of sign change

210   occurrences, around 10, tended to be lower than the non-sign change occurrences, which were approximately 20 events from evening to morning time. Nevertheless, there were some exceptional times during this period where the number of sign change occurrences exceeded the number of non-sign change occurrences, such as at 02:30 LT (20 sign change occurrences and 16 non-sign change occurrences) and 03:00 LT (22 sign change occurrences and 20 non-sign change occurrences).

215   The occurrences of both sign change and non-sign change remained relatively steady during the evening time until the morning time. However, the numbers of these two types of data started to increase around 10:00 LT, reaching their peak in the afternoon when the number of sign change occurrences began to surpass the number of non-sign change occurrences. The peak of non-sign change occurred at 12:30 LT with 84 events, gradually decreasing to around 20 events after 15:00 LT. On the other hand, the peak of sign change occurred at 13:30 LT with 113 events before decreasing and returning to their

220   approximate initial state after 19:00 LT. In the afternoon from 12:00 LT to 19:00 LT, the number of sign change occurrences consistently surpassed the number of non-sign change occurrences, especially after the peak of sign change, where the number of sign change events was twice as high as the number of non-sign change events. Notably, the higher number of both sign change and non-sign change occurrences between 10:00 LT and 19:00 LT indicates that the data from these hours

were not removed as frequently as the data from the rest of the evening to morning time, and in fact, contributed more to the

225   collective and available utilized data.
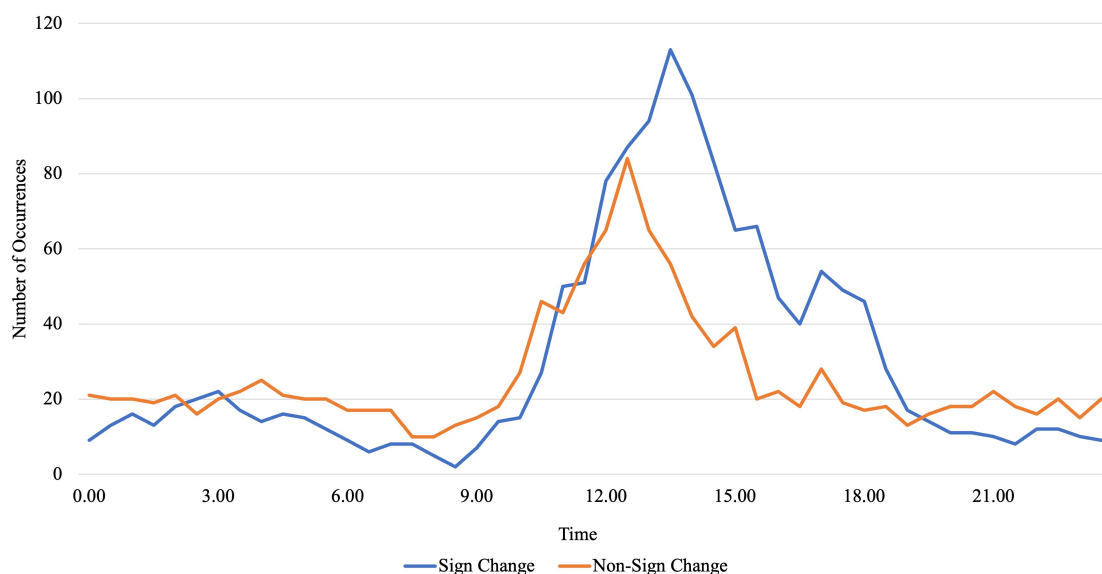
Figure 3: Quantification of sign change and non-sign change occurrences in a diel cycle.

230   The standard error of the mean for each category is lower during the sign change period compared to the non-sign change period. The difference in standard errors might be due to changes in the underlying data distribution during sign change period. During sign change, the data is more centered and tightly distributed. The presence of outliers or extreme values during non-sign change could lead to increased variability and larger standard errors. For $F_{c,0}$ (F_c), the average standard errors are 0.0051 (0.0059) µmol m^{-2} s^{-1} during sign change and 0.031 (0.034) µmol m^{-2} s^{-1} during non-sign change. The

235   corresponding average standard deviation values are 0.084 (0.086) µmol m^{-2} s^{-1} during sign change and 0.82 (0.90) µmol m^{-2} s^{-1} during non-sign change.

Moreover, these values further highlight the lower standard deviation of CO_2 flux and the environmental parameters during sign change periods, suggesting more consistent measurements during that time. Conversely, the standard deviation of CO_2

240   flux and those environmental parameters is higher during the non-sign change period. Specifically, during sign change, the standard deviation values for horizontal wind speed, vertical wind speed, temperature, molar density of dry air, and molar density of water vapor are 0.54 m s^{-1}, 0.013 m s^{-1}, 1.26 K, 0.23 mol m^{-3}, and 0.073 mol m^{-3}, respectively, while during non-sign change, they are 0.63 m s^{-1}, 0.014 m s^{-1}, 1.78 K, 0.28 mol m^{-3}, and 0.074 mol m^{-3}, respectively.

3.3 Positive-Negative Sign Change of the CO_2 Flux Due to WPL Correction

245   The sign change typically occurs when the raw CO_2 flux is small and close to equilibrium. On average, the mean value of $F_{c,0}$ during the sign change is -0.11 μmol m^{-2} s^{-1}, whereas the mean value for $F_{c,0}$ during the non-sign change is -0.169 μmol m^{-2} s^{-1}. In comparison, the mean value of F_c during the sign change is 0.074 μmol m^{-2} s^{-1}, while during the non-sign change it is -0.096 μmol m^{-2} s^{-1}.

250   Based on the mean differences calculated as $(F_{c,0} - F_c)/F_{c,0}$, the overall sign change CO_2 fluxes are significantly different from zero (p-value < 0.01), including for lower CO_2 flux values near zero, specifically below 0.05 μmol m^{-2} s^{-1}. The differences for overall sign change CO_2 fluxes were found to be $2.47 \pm 3.56\%$ (mean $\pm$ 95% confidence interval), and for sign change CO_2 fluxes with magnitude below 0.05 μmol m^{-2} s^{-1}, they were $3.47 \pm 2.53\%$. Furthermore, the t-test results consistently demonstrated that CO_2 flux values during sign change events were significantly different (p-value < 0.01) from

255   those observed during non-sign change events, even within flux values close to zero. These findings highlight the statistical evidence for the significance of sign change phenomena in this research.

During the study period, the cumulative value of the second term, the third term, and the fourth term in the WPL correction has an average value of 0.15 μmol m^{-2} s^{-1}. Additionally, the accumulation of these terms in the WPL correction

260   demonstrates a higher value during the sign change period compared to the non-sign change period, with average values of 0.187 μmol m^{-2} s^{-1} and 0.105 μmol m^{-2} s^{-1}, respectively.

Among these three terms, the two largest correction values are attributed to temperature and water vapor fluctuations, which are represented by the second term and the third term, respectively. The third term of the WPL correction is the primary

265   component and the most influential factors in altering the sign of CO_2 flux when applying the WPL correction. In contrast, the correction for pressure fluctuations, the fourth term, has the least significant effect. The average values for the second term, the third term, and the fourth term of the WPL correction are -0.0141 μmol m^{-2} s^{-1}, 0.168 μmol m^{-2} s^{-1}, -0.00336 μmol m^{-2} s^{-1}, respectively.

270   The WPL formula consists of several parameters, including vertical wind speed, temperature, molar density of water vapor, molar density of dry air, and pressure. The average values for each parameter are 0.019 m s^{-1}, 302.41 K, 1.24 mol m^{-3}, 38.79 mol m^{-3}, and 100.74 kPa, respectively. Each term in the WPL correction is determined by a different parameter, with the common factor being the vertical wind speed in each term. The vertical wind speed is the main parameter in the WPL formula.

275

According to Eq. (1), a higher (lower) vertical wind speed can result in a higher (lower) value for the WPL correction. Notably, the average value of vertical wind speed during the sign change period is 0.0211 m s^{-1}, which is higher than during the non-sign change period, which has an average of 0.0175 m s^{-1}. The results of the t-test also indicate a significant difference (p-value < 0.01) in mean vertical wind speed values between the groups categorized by sign changes and those

280   without sign changes. Therefore, vertical wind speed can be one of the factors contributing to the sign change of the CO_2 flux.

The vertical wind speed can be influenced by the horizontal wind speed since the two are interconnected. During the study period, the average value of horizontal wind speed is 0.92 m s^{-1}. Similar to the vertical wind speed, the horizontal wind

285   speed during the sign change period (average of 1.05 m s^{-1}) is higher compared to the non-sign change period (average of 0.77 m s^{-1}). The t-test analysis also reveals a significant difference in mean horizontal wind speed values between the sign change and non-sign change groups, indicating statistical significance (p-value < 0.01).

3.4 The Correction for Temperature Fluctuations of WPL on CO_2 Flux Sign Change

The correction for temperature fluctuations in the WPL formula, specifically the second term of the WPL correction, is

290   determined by temperature and vertical wind speed. These two factors play a crucial role in determining the second term of the WPL correction value, which can influence the sign of the CO_2 flux. The second term is directly proportional to the vertical wind speed but inversely proportional to the temperature. A higher (lower) temperature results in a lower (higher) value for the second term of the WPL correction, while a higher (lower) vertical wind speed leads to a higher (lower) value for the second term of the WPL correction.

295

During sign changes, the average value from the second term of the WPL correction is –0.00678 µmol m^{-2} s^{-1}, which is higher than the average value during non-sign changes, which is –0.0224 µmol m^{-2} s^{-1}. The t-test results also indicate a significant difference (p-value < 0.01) in the mean values when comparing the sign change group to the non-sign change group. This suggests that the average value from the second term of the WPL correction during sign changes has a greater

300   influence on changing the sign of the CO_2 flux from negative to positive.

The average temperature values during sign changes and non-sign changes are 302.65 K and 302.02 K, respectively. According to a t-test (with a p-value less than 0.01), there is a significant distinction in mean temperature values between the groups that experienced sign changes and those that did not. The higher (lower) temperature during the sign change (non-

305   sign change) period can be the main reason for the lower (higher) absolute value of the second term WPL correction.

Additionally, horizontal wind speed may impact temperature. During sign changes, there is a statistically significant negative correlation between horizontal wind speed and temperature (Pearson correlation coefficient, r = –0.25). As horizontal wind

310 speed increases (or decreases), temperature decreases (or increases), which can suggest a cooling effect on the surface air temperature. In this scenario, a higher horizontal wind speed can lead to a higher vertical wind speed, resulting in a higher value for the second term of the WPL correction. Furthermore, the lower temperature caused by higher horizontal wind speed can contribute to a higher value for the second term of the WPL correction.

315 In contrast to the sign change period, the correlation between horizontal wind speed and temperature during the non-sign change is statistically significant and positive (r = 0.11). This means that as horizontal wind speed increases (or decreases), temperature also increases (or decreases) during the non-sign change. The lower horizontal wind speed during the non-sign change may have a lesser effect on decreasing temperature, leading to the positive correlation between horizontal wind speed and temperature.

3.5 The Correction for Water Vapor Fluctuations of WPL on CO_2 Flux Sign Change

320 The correction for water vapor fluctuations in the WPL formula (the third term of the WPL correction) is determined by the molar density of H_2O, the molar density of dry air, and the vertical wind speed. The third term is directly proportional to the vertical wind speed but inversely proportional to the molar density of dry air. Lower molar density of dry air and higher vertical wind speed can result in a higher value for the third term of the WPL correction, potentially causing a sign change in the CO_2 flux. The average value of the third term of the WPL correction during sign changes is 0.196 μmol m^{-2} s^{-1}, which is

325 significantly higher than during non-sign changes (0.136 μmol m^{-2} s^{-1}; p-value < 0.01).

The Ideal Gas Law and Dalton's law related to the behavior of gas mixtures, specifically the partial pressures and molar densities of water vapor and dry air, demonstrate the inverse relationship between molar density of H_2O and molar density of dry air (Miller et al., 2010; Ahrens, 2015). A higher (lower) molar density of H_2O can lead to a lower (higher) molar density

330 of dry air due to the corresponding increase (decrease) in the partial pressure of water vapor and the decrease (increase) in the partial pressure of dry air.

Temperature may play a role in the relationship between the molar density of H_2O and the molar density of dry air, as temperature has an inverse relationship with the molar density of H_2O due to the ideal gas law, where higher temperatures

335 result in increased kinetic energy, causing gas molecules to occupy larger volumes and decreasing molar density (Andrews, 2010; Atkins and De Paula, 2006). The average molar density of H_2O is lower during sign changes (1.24 mol m^{-3}) compared to non-sign changes (1.25 mol m^{-3}), which is opposite to the trend observed in temperature. The mean molar density of H_2O also exhibits a significant difference between the sign change group and the non-sign change group, as indicated by the t-test (p-value < 0.01).

340

The formulation of the molar density of dry air demonstrates an inverse relationship with temperature, where a higher (lower) temperature can result in a lower (higher) partial pressure of dry air. In contrast to temperature, but consistent with the molar density of H_2O, the molar density of dry air exhibits significant differences during sign changes (average of 38.7 mol m^{-3}) compared to non-sign changes (average of 38.8 mol m^{-3}; p-value < 0.01). Consequently, higher temperatures can

345   further increase the value of the third term in the WPL formula by decreasing the molar density of dry air.

Horizontal wind speed and temperature can influence the molar density of water vapor and dry air during sign change periods. In this period, a negative correlation exists between horizontal wind speed and temperature. Higher wind speed can cause lower temperatures, which, in turn, can result in higher molar density of dry air.

350

Horizontal wind speed can influence the molar density of water vapor through the advection process by causing the horizontal movement of air masses with varying water vapor content. A statistically significant negative correlation (r = –0.15) was observed during sign changes, indicating higher (lower) horizontal wind speed associated with lower (higher) water vapor molar density. Notably, horizontal wind speed is higher during sign changes compared to non-sign change

355   periods, in contrast to water vapor molar density. This wind speed influence on water vapor density subsequently can affect the molar density of dry air, leading to a positive correlation between wind speed and dry air density during sign changes (r = 0.17; p-value < 0.01).

During the non-sign change period, a statistically significant negative correlation persists between horizontal wind speed and

360   the molar density of water vapor (r = –0.26). However, the correlation between horizontal wind speed and the molar density of dry air is weak and not statistically significant (r = 0.05). The absence of a statistically significant correlation between wind speed and dry air molar density in this period could be attributed to a stronger influence of temperature on dry air molar density.

365   Atmospheric pressure also plays a role in determining the molar density of dry air (Andrews, 2010; Atkins and De Paula, 2006; Ahrens, 2015). Higher (lower) pressure can lead to a higher (lower) molar density of dry air. Notably, the sign change period average pressure (100.73 kPa) is significantly lower compared to the non-sign change period (100.75 kPa; p-value < 0.01). A lower pressure can cause a decrease in the molar density of dry air, subsequently increasing the value of the third term in the WPL formula.

370   **3.6 Diel Cycle Analysis of WPL Correction Parameters and Their Relationships**

The diel cycle presented in Fig. 4 provides more insights into the parameters involved in the WPL correction. Initially, the diel cycle reveals that vertical wind speed reaches its lowest values, less than 0.02 m s^{-1}, around noon, while its peak, over

0.028 m s^{-1}, occurs around 03:00 LT and 22:00 LT. The vertical wind speed decreases from around 03:00 LT until approximately noon and then starts to increase in the afternoon until around 22:00 LT.

375

The diel cycle pattern of vertical wind speed is similar to that of the second term and the fourth term of the WPL correction, showing a direct proportionality to these two terms. The diel cycle of the second term of the WPL correction fluctuates within a range of –0.07 µmol m^{-2} s^{-1} to 0.06 µmol m^{-2} s^{-1}. The lower values are observed during the daytime, particularly negative values between 08:00 LT and 19:00 LT, while the rest of the time corresponds to positive values of the second term

380 WPL correction. On the other hand, the fourth term tends to produce negative values, especially during the daytime, where the values can drop to less than –0.006 µmol m^{-2} s^{-1}. From 19:00 LT until 08:00 LT, the values for the fourth term WPL correction are around 0 µmol m^{-2} s^{-1}, and they decrease until around 10:00 LT to less than –0.007 µmol m^{-2} s^{-1} before starting to increase again from around 16:00 LT until 20:00 LT.

385 The diel cycle pattern of vertical wind speed also aligns with that of horizontal wind speed, which ranges from 0.7 m s^{-1} to 1.3 m s^{-1}, but exhibits the opposite trend compared to temperature. Temperature reaches its highest values during the daytime, increasing in the morning after 06:00 LT and decreasing after 18:00 LT. This emphasizes the direct proportionality between vertical wind speed and the second term WPL correction, as well as the inverse relationship between temperature and the second term WPL correction in the formula.

390
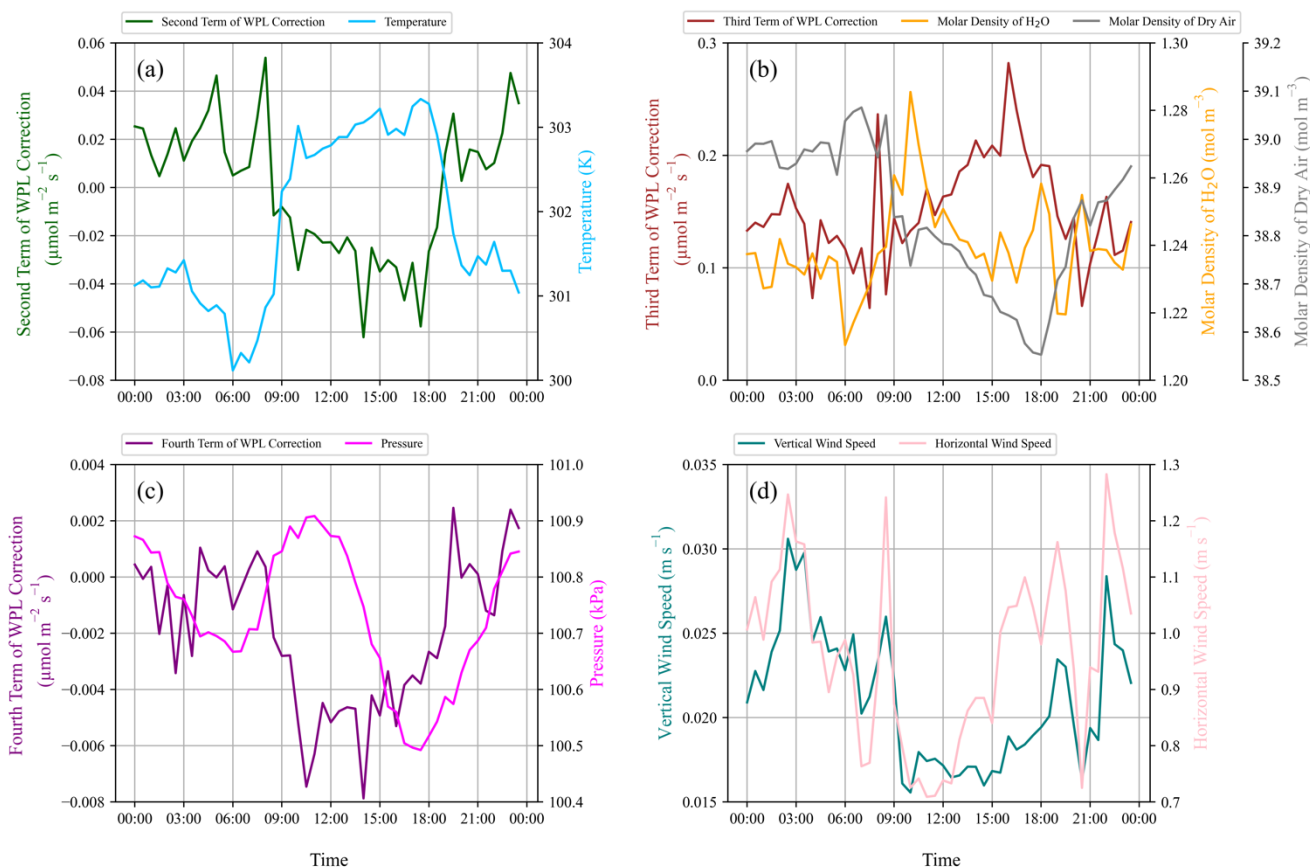
Figure 4: The climatological variation of diel atmospheric parameters in 2016: (a) Second term of WPL correction and temperature, (b) Third term of WPL correction, molar density of H₂O, and molar density of dry air, (c) Fourth term of WPL correction and pressure, and (d) horizontal wind speed and vertical wind speed.

395

The fourth term of the WPL correction follows a similar trend to the vertical wind speed; however, the influence of pressure on the fourth term of the WPL correction is observed between 03:00 LT and 18:00 LT, exhibiting an inverse relationship with pressure during these hours. During the early morning hours, the pressure experiences a slight decrease from approximately 100.87 kPa to less than 100.7 kPa. As the day progresses, the pressure gradually increases, reaching over

400   100.9 kPa around 11:00 LT. After reaching its peak, the pressure decreases to around 100.5 kPa in the afternoon and then increases again before 18:00 LT, surpassing 100.8 kPa at around 10:00 LT.

Unlike the second term and fourth term of the WPL correction, the third term always has positive values throughout the diel cycle, with higher values during the day. The third term increases before 09:00 LT and reaches a peak of over 0.2 μmol m^{-2}

405   s^{-1} around 16:00 LT before decreasing to below 0.1 μmol m^{-2} s^{-1} before 21:00 LT. The diel trend of the third term tends to

15

be opposite to diel trends of the molar density of H_2O and molar density of dry air, especially during the daytime. It seems that the lower molar density of dry air leads to higher values of the third term WPL correction, contributing to the sign change of the CO_2 flux. Based on Fig. 3, sign change occurrences are more frequent after 11:00 LT until 19:00 LT, when the third term of the WPL correction is higher and the molar density of dry air is lower. Temperature might also contribute to the

410   molar density of dry air during this time, as higher temperatures during the day can lead to a lower molar density of dry air. This indicates that the third term of the WPL correction and molar density of dry air are the main reasons for the sign change of the CO_2 flux during the daytime, considering that the second term, fourth term, and vertical wind speed are lower during this time.

415   During times other than between 11:00 LT and 19:00 LT, when the number of sign change occurrences is lower, the molar density of dry air is not as low as between 11:00 LT and 19:00 LT, but the value of the third term of the WPL correction remains positive, around 0.1 $\mu mol\ m^{-2}\ s^{-1}$. This suggests that the third term of the WPL correction can still contribute to the sign change of the CO_2 flux during times other than between 11:00 LT and 19:00 LT. In contrast to the period between 11:00 LT and 19:00 LT, vertical wind speed is higher during these times, which also leads to higher values of the second term and

420   fourth term of the WPL correction, and the temperature is lower, potentially further increasing the second term of the WPL correction within the range of 0 $\mu mol\ m^{-2}\ s^{-1}$ and 0.06 $\mu mol\ m^{-2}\ s^{-1}$.

3.7 CO_2 Flux Data with Quality Flagging of the WPL Correction

Based on QF_{WPL}, there are a total of 691 data (24.92%) for $|QF_{WPL}| \leq 0.5$ ($QF_{WPL,1}$), 334 data (12.04%) for $0.5 < |QF_{WPL}| \leq 1$ ($QF_{WPL,2}$), and 1748 data (63.04%) for $|QF_{WPL}| > 1$ ($QF_{WPL,3}$). As shown in Fig. 5, fluctuations are evident in all three

425   variables throughout the day. The number of CO_2 fluxes with $QF_{WPL,1}$ varies, with a minimum of 4 and a maximum of 34. CO_2 fluxes with $QF_{WPL,2}$ range from 0 to 31, while CO_2 fluxes with $QF_{WPL,3}$ range from 9 to 131. Noticeable patterns emerge in the data, with certain periods of the day displaying higher values in all three variables.
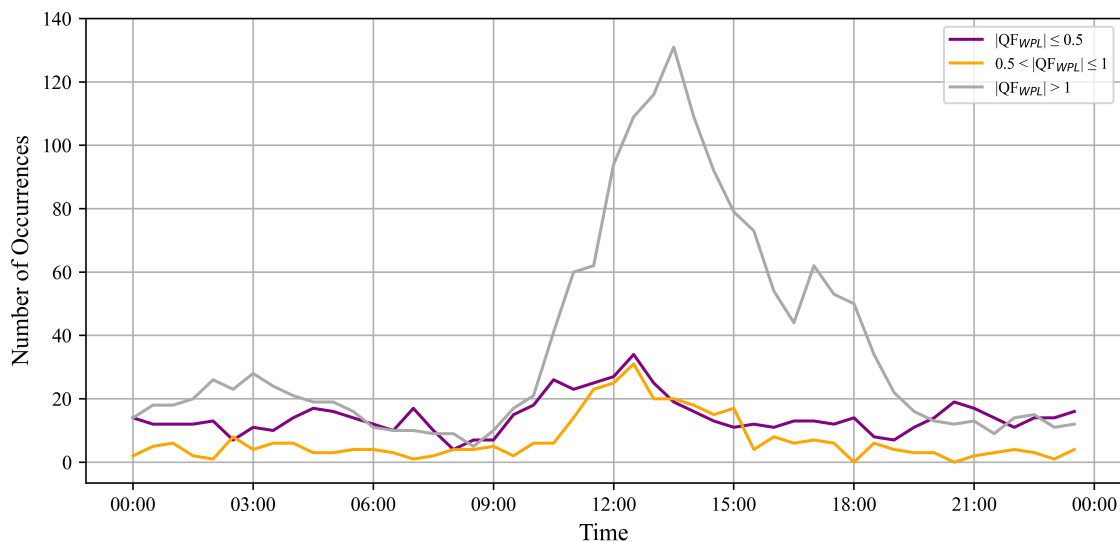
Figure 5: The QF$_{WPL}$ category occurrences throughout a diel cycle.

The difference value between QF$_{WPL,3}$ and both QF$_{WPL,1}$ and QF$_{WPL,2}$ is more significant during the daytime than at night, especially at the peak of QF$_{WPL,3}$, although QF$_{WPL,3}$ also surpasses both QF$_{WPL,1}$ and QF$_{WPL,2}$ between 01:30 LT and 04:00 LT. The frequency of occurrences for QF$_{WPL,1}$ and QF$_{WPL,2}$ begins to increase at 08:00 LT (4 instances), peaking at 12:30 LT (more than 30 occurrences). Meanwhile, the number for QF$_{WPL,3}$ starts increasing at 08:30 LT (5 events) and peaks at 13:30 LT (131 events), subsequently dropping to below 20 occurrences after 19:00 LT. These significant QF$_{WPL,3}$ occurrences during the day coincide with higher occurrences of sign change CO_2 flux.

Fig. 6a shows the numbers of F_c within $|QF_{WPL}| \leq 1$, excluding F_c with $|QF_{WPL}| > 1$ and representing WPL-corrected CO_2 fluxes that are considered good and very good based on the quality flagging of the WPL correction. Within $|QF_{WPL}| \leq 1$, 98.38% of the data are non-sign change fluxes. Based on the figure, CO_2 fluxes within $|QF_{WPL}| \leq 1$ are predominantly non-sign change fluxes. Nevertheless, there are still some sign change CO_2 fluxes observed between 11:30 LT and 18:30 LT, which can suggest that not all sign change fluxes are errors.

Additionally, within $|QF_{WPL}| > 1$, 83.37% of the data consists of sign change fluxes, while 16.63% represents non-sign change fluxes. Figure 6b, displaying F_c values within $|QF_{WPL}| > 1$, reveals a predominance of sign change CO_2 fluxes, especially during the daytime. Although the number of sign change CO_2 fluxes is consistently higher than the non-sign change fluxes throughout the period characterized by $|QF_{WPL}| > 1$, it is noteworthy that non-sign change fluxes are still observed. Similar to the sign change CO_2 fluxes, the peak of non-sign change CO_2 fluxes also occurs in the afternoon.
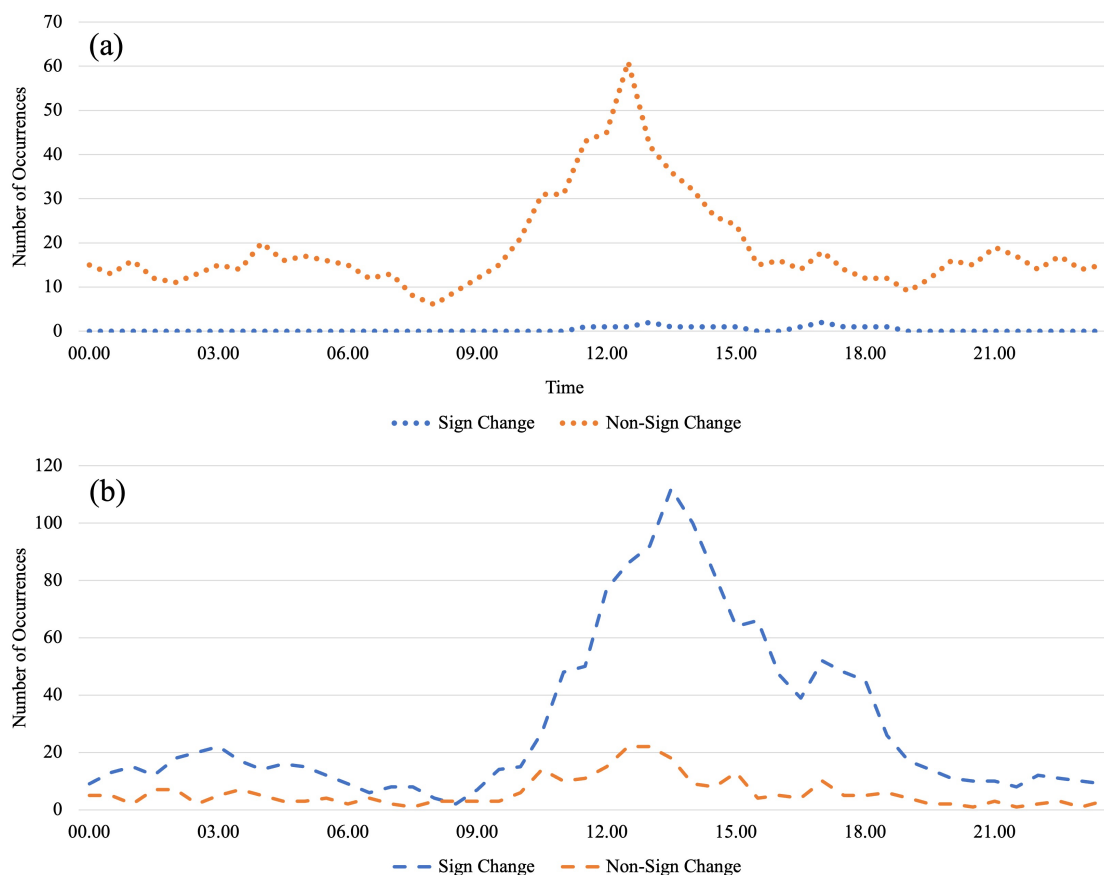
Figure 6: Quantification of sign change and non-sign change occurrences in a diel cycle within (a) $|QF_{WPL}| \leq 1$ and (b) $|QF_{WPL}| > 1$.

As the CO_2 flux for $|QF_{WPL}| \leq 1$ tends to exclude sign change fluxes, the CO_2 flux within $|QF_{WPL}| \leq 1$ exhibits more negative CO_2 flux than the fluxes prior to the QF_{WPL} implementation, as illustrated in Fig. 7. Additionally, positive CO_2 fluxes are still visible during the day for both $F_{c,0}$ and F_c within $|QF_{WPL}| \leq 1$. In comparison, F_c during $|QF_{WPL}| \leq 1$ demonstrates more pronounced positive and negative CO_2 fluxes.

In the case of $|QF_{WPL}| \leq 1$, the average values of $F_{c,0}$ and F_c were -0.185 µmol m^{-2} s^{-1} and -0.155 µmol m^{-2} s^{-1}, respectively, both of which represent stronger negative fluxes compared to the fluxes prior to the QF_{WPL} implementation (-0.16 µmol m^{-2} s^{-1} and -0.037 µmol m^{-2} s^{-1}, respectively). By excluding F_c with $|QF_{WPL}| > 1$, the difference between F_c and $F_{c,0}$ within $|QF_{WPL}| \leq 1$ decreases over time, narrowing to a range of 0–0.15 µmol m^{-2} s^{-1}. Prior to implementing QF_{WPL}, there was a noticeable increase in the difference at 08:00 LT compared to other times. Compared to the fluxes before implementing

18

465   QF_{WPL}, the difference between F_c and $F_{c,0}$ within $|QF_{WPL}| \leq 1$ at 08:00 LT decreased by 0.188 µmol m^{-2} s^{-1} to 0.1 µmol m^{-2} s^{-1} (35% of the fluxes before QF_{WPL} implementation).
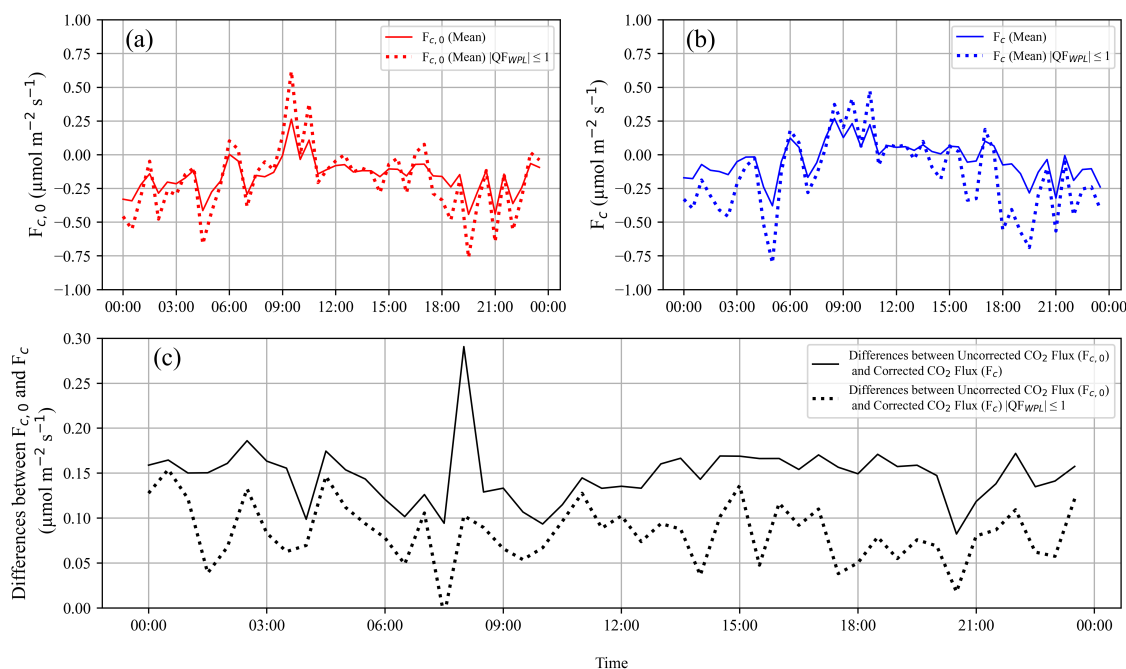
Figure 7: The climatological variation of diel (a) $F_{c,0}$, (b) F_c, and (c) difference value between $F_{c,0}$ and F_c, with the
470   **corresponding variables within $|QF_{WPL}| \leq 1$.**

The decrease in the difference between F_c and $F_{c,0}$ can be attributed to the lower absolute values of vertical wind speed, as well as the second and third terms of the WPL correction. At 08:00 LT, the average values within $|QF_{WPL}| \leq 1$ were as follows: vertical wind speed, 0.012 m s^{-1}; second term correction, 0.0016 µmol m^{-2} s^{-1}; and third term correction, 0.1 µmol
475   m^{-2} s^{-1}. These values represented 51%, 3%, and 42% of the respective values before the QF_{WPL} implementation, and they were also lower by 0.011 m s^{-1}, 0.052 µmol m^{-2} s^{-1}, and 0.14 µmol m^{-2} s^{-1}, respectively. Additionally, the CO_2 flux at 08:00 LT also decreased. Prior to the QF_{WPL} implementation, $F_{c,0}$ was –0.16 µmol m^{-2} s^{-1}, while F_c was 0.13 µmol m^{-2} s^{-1}. Within $|QF_{WPL}| \leq 1$, $F_{c,0}$ and F_c were lower by 0.11 µmol m^{-2} s^{-1} and 0.08 µmol m^{-2} s^{-1}, respectively, attaining –0.05 µmol m^{-2} s^{-1} and 0.05 µmol m^{-2} s^{-1}.

480

Nonetheless, the need to specially check CO_2 fluxes within $|QF_{WPL}| > 1$ does not necessarily imply an error in CO_2 flux measurement, and it might suggest further research into validating the application of the WPL correction to small CO_2 fluxes, especially on sign-changing CO_2 fluxes and fluxes requiring a check based on the QF_{WPL}. The verification and

validation process can involve a comparison with CO_2 flux measurements obtained using a closed-path gas analyzer, which
485   is a limitation in this study. It is worth noting that achieving complete isothermal conditions in the measurement volume of
the closed-path sensor in the closed-path gas analyzer is essential to obtain the most accurate fluxes at CO_2 fluxes < 5 μmol
$m^{-2}\ s^{-1}$, as suggested by Jentzsch et al. (2021).

4 Conclusions

A comprehensive analysis of CO_2 flux patterns at the tropical coast reveals a dynamic flux characterized by fluctuating
490   magnitudes and exhibiting periods of CO_2 emissions and CO_2 uptakes, where the coastal waters predominantly act as a sink.
The diel cycle showed fluctuations in the CO_2 flux, with smaller magnitudes during the daytime and greater uptake
movements during the nighttime.

The application of the Webb-Pearman-Leuning (WPL) correction resulted in changes in the sign of the CO_2 flux, indicating a
495   shift from CO_2 sink to CO_2 source. Sign changes occur frequently, accounting for over half of the available data, with a
substantial number of sign change events during the afternoon hours. The different results obtained from these fluxes can
significantly impact the conclusion regarding carbon exchange at the studied location.

The WPL correction parameters, particularly the second and third terms, play crucial roles in CO_2 flux sign changes. Higher
500   vertical wind speed and lower temperature contribute to the second term of the correction for temperature fluctuations.
Particularly, the lower molar density of dry air and higher vertical wind speed contribute to the third term related to water
vapor fluctuations, which is the major reason for the sign change of the CO_2 flux. The diel cycle analysis further reveals the
presence of positive values in the third term of the WPL correction throughout the day, with higher values during the
daytime that cause more occurrences of sign changes in the CO_2 flux.
505

The analysis of QF_{WPL} highlights that the majority of CO_2 flux data falls within the $|QF_{WPL}| > 1$ category. The difference
between $|QF_{WPL}| > 1$ and both $|QF_{WPL}| \leq 0.5$ and $0.5 < |QF_{WPL}| \leq 1$ is notably more pronounced during the daytime. $|QF_{WPL}| > 1$ predominantly exhibits sign change fluxes, especially during the day, coinciding with an increase in instances of sign
change in CO_2 flux. Within $|QF_{WPL}| \leq 1$, most of the data comprises non-sign change fluxes, while occasional sign change
510   fluxes persist. The implementation of QF_{WPL} within $|QF_{WPL}| \leq 1$ results in lower values of the WPL correction, especially in
terms of vertical wind speed as well as the second and third terms of the WPL correction, ultimately leading to a stronger
negative CO_2 flux within this study location.

Further research may involve CO_2 flux measurement using a closed-path gas analyzer for a more comprehensive
515   investigation and verification of the application of the WPL correction to small CO_2 flux in the coastal sea environment.

Specifically, it could focus on assessing the accuracy and reliability of sign-changing CO_2 flux, especially fluxes requiring a check based on the quality flagging associated with the WPL correction.

Data Availability

The study made use of data acquired from the Muka Head Station, located at the Centre for Marine and Coastal Studies of
520 Universiti Sains Malaysia. This data can be accessed through the following website: http://atmosfera.usm.my/api.html.

Author Contribution

All authors contributed in the conception and design of the study. MFS initiated the research, devised the methodology, performed data analysis, and produced all the figures for the paper, along with the initial writing. YY contributed to the interpretation of the results and offered valuable insights for the writing and reviewing process of the manuscript. AES,
525 HMA, and EJJ provided essential resources to facilitate the research, including data collection and curation. The final manuscript was read and approved by all authors.

Competing Interests

The authors declare that they have no conflict of interest.

Acknowledgements

Financial Support

References

Aalto, N. J., Campbell, K., Eilertsen, H. C., and Bernstein, H. C.: Drivers of Atmosphere-Ocean CO_2 Flux in Northern
540 Norwegian Fjords, Front Mar Sci, 8, https://doi.org/10.3389/fmars.2021.692093, 2021.

Ahrens, C. D.: Meteorology today: an introduction to weather, climate, and the environment, Cengage Learning Canada Inc,
  2015.

Andrews, D. G.: An Introduction to Atmospheric Physics, 2nd ed., Cambridge University Press,
  https://doi.org/10.1017/CBO9780511800788, 2010.

545 Atkins, P. and De Paula, J.: Physical chemistry, Macmillan, 2006.

Borges, A. v., Delille, B., and Frankignoulle, M.: Budgeting sinks and sources of CO_2 in the coastal ocean: Diversity of
  ecosystem counts, Geophys Res Lett, 32, 1–4, https://doi.org/10.1029/2005GL023053, 2005.

Broecker, W. S., Ledwell, J. R., Takahashi, T., Weiss, R., Merlivat, L., Memery, L., Peng, T.-H., Jahne, B., and Munnich, K.
  O.: Isotopic versus micrometeorologic ocean CO_2 fluxes: A serious conflict , J Geophys Res, 91, 10517,
550 https://doi.org/10.1029/jc091ic09p10517, 1986.

Burba, G., McDermitt, D. K., Grelle, A., Anderson, D. J., and Xu, L.: Addressing the influence of instrument surface heat
  exchange on the measurements of CO_2 flux from open-path gas analyzers, Glob Chang Biol, 14, 1854–1876,
  https://doi.org/10.1111/j.1365-2486.2008.01606.x, 2008.

Burba, G., Schmidt, A., Scott, R. L., Nakai, T., Kathilankal, J., Fratini, G., Hanson, C., Law, B., Mcdermitt, D. K., Eckles,
555 R., Furtaw, M., and Velgersdyk, M.: Calculating CO_2 and H_2O eddy covariance fluxes from an enclosed gas analyzer
  using an instantaneous mixing ratio, Glob Chang Biol, 18, 385–399, https://doi.org/10.1111/j.1365-2486.2011.02536.x,
  2012.

Burba, G., Madsen, R., and Feese, K.: Eddy covariance method for CO_2 emission measurements in CCUS applications:
  Principles, instrumentation and software, in: Energy Procedia, 329–336, https://doi.org/10.1016/j.egypro.2013.08.038,
560 2013.

Chien, H., Zhong, Y. Z., Yang, K. H., and Cheng, H. Y.: Diurnal variability of CO_2 flux at coastal zone of Taiwan based on
  eddy covariance observation, Cont Shelf Res, 162, 27–38, https://doi.org/10.1016/j.csr.2018.04.006, 2018.

Doney, S. C., Tilbrook, B., Roy, S., Metzl, N., le Quéré, C., Hood, M., Feely, R. A., and Bakker, D.: Surface-ocean CO_2
  variability and vulnerability, Deep Sea Res 2 Top Stud Oceanogr, 56, 504–511,
565 https://doi.org/10.1016/j.dsr2.2008.12.016, 2009.

Edson, J. B., Fairall, C. W., Bariteau, L., Zappa, C. J., Cifuentes-Lorenzen, A., McGillis, W. R., Pezoa, S., Hare, J. E., and
  Helmig, D.: Direct covariance measurement of CO_2 gas transfer velocity during the 2008 Southern Ocean Gas Exchange
  Experiment: Wind speed dependency, J Geophys Res Oceans, 116, https://doi.org/10.1029/2011JC007022, 2011.

Else, B. G. T., Papakyriakou, T. N., Galley, R. J., Drennan, W. M., Miller, L. A., and Thomas, H.: Wintertime CO_2 fluxes in
an Arctic polynya using eddy covariance: Evidence for enhanced air-sea gas transfer during ice formation, J Geophys
Res Oceans, 116, https://doi.org/10.1029/2010JC006760, 2011.

Foken, T., Leuning, R., Oncley, S. R., Mauder, M., and Aubinet, M.: Corrections and Data Quality Control, in: Eddy
Covariance, Springer Netherlands, Dordrecht, 85–131, https://doi.org/10.1007/978-94-007-2351-1_4, 2012.

Foken, Th. and Wichura, B.: Tools for quality assessment of surface-based flux measurements, Agric For Meteorol, 78, 83–
105, https://doi.org/10.1016/0168-1923(95)02248-1, 1996.

Gutiérrez-Loza, L. and Ocampo-Torres, F. J.: Air-sea CO_2 fluxes measured by eddy covariance in a coastal station in Baja
California, México, in: IOP Conference Series: Earth and Environmental Science, https://doi.org/10.1088/1755-
1315/35/1/012012, 2016.

He, Y., Yang, J., Zhuang, Q., Harden, J. W., McGuire, A. D., Liu, Y., Wang, G., and Gu, L.: Incorporating microbial
dormancy dynamics into soil decomposition models to improve quantification of soil carbon dynamics of northern
temperate forests, J Geophys Res Biogeosci, 120, 2596–2611, https://doi.org/10.1002/2015JG003130, 2015.

Heimsch, L., Lohila, A., Tuovinen, J. P., Vekuri, H., Heinonsalo, J., Nevalainen, O., Korkiakoski, M., Liski, J., Laurila, T.,
and Kulmala, L.: Carbon dioxide fluxes and carbon balance of an agricultural grassland in southern Finland,
Biogeosciences, 18, 3467–3483, https://doi.org/10.5194/bg-18-3467-2021, 2021.

Ikawa, H., Faloona, I., Kochendorfer, J., Paw U, K. T., and Oechel, W. C.: Air-sea exchange of CO_2 at a Northern California
coastal site along the California Current upwelling system, Biogeosciences, 10, 4419–4432, https://doi.org/10.5194/bg-
10-4419-2013, 2013.

Jentzsch, K., Boike, J., and Foken, T.: Importance of the Webb, Pearman, and Leuning (WPL) correction for the
measurement of small CO2 fluxes, Atmos Meas Tech, 14, 7291–7296, https://doi.org/10.5194/amt-14-7291-2021, 2021.

Jones, E. P. and Smith, S. D.: A first measurement of sea-air CO_2 flux by eddy correlation, J Geophys Res, 82, 5990–5992,
https://doi.org/10.1029/jc082i037p05990, 1977.

Kondo, F. and Tsukamoto, O.: Air-Sea CO_2 Flux by Eddy Covariance Technique in the Equatorial Indian Ocean, Journal of
Oceanography, 449–456 pp., 2007.

Liebethal, C. and Foken, T.: On the Significance of the Webb Correction to Fluxes, Boundary Layer Meteorol, 109, 99–106,
2003.

Lokupitiya, E., Denning, A. S., Schaefer, K., Ricciuto, D., Anderson, R., Arain, M. A., Baker, I., Barr, A. G., Chen, G.,
Chen, J. M., Ciais, P., Cook, D. R., Dietze, M., el Maayar, M., Fischer, M., Grant, R., Hollinger, D., Izaurralde, C., Jain,
A., Kucharik, C., Li, Z., Liu, S., Li, L., Matamala, R., Peylin, P., Price, D., Running, S. W., Sahoo, A., Sprintsin, M.,
Suyker, A. E., Tian, H., Tonitto, C., Torn, M., Verbeeck, H., Verma, S. B., and Xue, Y.: Carbon and energy fluxes in
cropland ecosystems: a model-data comparison, Biogeochemistry, 129, 53–76, https://doi.org/10.1007/s10533-016-0219-
3, 2016.

Massman, W. J. and Tuovinen, J.-P.: An Analysis and Implications of Alternative Methods of Deriving the Density (WPL) Terms for Eddy Covariance Flux Measurements, Boundary Layer Meteorol, 121, 221–227, https://doi.org/10.1007/s10546-006-9070-8, 2006.

605 Mauder, M., Cuntz, M., Drüe, C., Graf, A., Rebmann, C., Schmid, H. P., Schmidt, M., and Steinbrecher, R.: A strategy for quality and uncertainty assessment of long-term eddy-covariance measurements, Agric For Meteorol, 169, 122–135, https://doi.org/10.1016/j.agrformet.2012.09.006, 2013.

Mauder, M., Foken, T., Aubinet, M., and Ibrom, A.: Eddy-Covariance Measurements, 1473–1504, https://doi.org/10.1007/978-3-030-52171-4_55, 2021.

610 McGowan, H. A., MacKellar, M. C., and Gray, M. A.: Direct measurements of air-sea CO_2 exchange over a coral reef, Geophys Res Lett, 43, 4602–4608, https://doi.org/10.1002/2016GL068772, 2016.

Miller, S. D., Marandino, C., and Saltzman, E. S.: Ship-based measurement of air-sea CO_2 exchange by eddy covariance, Journal of Geophysical Research Atmospheres, 115, https://doi.org/10.1029/2009JD012193, 2010.

Nakai, Y., Matsuura, Y., Kajimoto, T., Abaimov, A. P., Yamamoto, S., and Zyryanova, O. A.: Eddy covariance CO_2 flux
615 above a Gmelin larch forest on continuous permafrost in Central Siberia during a growing season, Theor Appl Climatol, 93, 133–147, https://doi.org/10.1007/s00704-007-0337-x, 2008.

Prytherch, J., Yelland, M. J., Pascal, R. W., Moat, B. I., Skjelvan, I., and Neill, C. C.: Direct measurements of the CO_2 flux over the ocean: Development of a novel method, Geophys Res Lett, 37, https://doi.org/10.1029/2009GL041482, 2010.

Rey-Sánchez, A. C., Bohrer, G., Morin, T. H., Shlomo, D., Mirfenderesgi, G., Gildor, H., and Genin, A.: Evaporation and
620 CO_2 fluxes in a coastal reef: an eddy covariance approach, Ecosystem Health and Sustainability, 3, https://doi.org/10.1080/20964129.2017.1392830, 2017.

Stull, R. B.: An Introduction to Boundary Layer Meteorology, https://doi.org/https://doi.org/10.1007/978-94-009-3027-8, 1988.

Tokoro, T. and Kuwae, T.: Improved post-processing of eddy-covariance data to quantify atmosphere-aquatic ecosystem
625 CO_2 Exchanges, Front Mar Sci, 5, https://doi.org/10.3389/fmars.2018.00286, 2018.

Wanninkhof, R.: Relationship Between Wind Speed and Gas Exchange Over the Ocean, JOURNAL OF GEOPHYSICAL RESEARCH, 1992.

Wanninkhof, R., Asher, W. E., Ho, D. T., Sweeney, C., and McGillis, W. R.: Advances in quantifying air-sea gas exchange and environmental forcing, https://doi.org/10.1146/annurev.marine.010908.163742, 2009.

630 Webb, E. K., Pearman, G. I., and Leuning, R.: Correction of flux measurements for density effects due to heat and water vapour transfer, 85–100 pp., 1980.

Yusup, Y., Kayode, J. S., and Alkarkhi, A. F. M.: Data on micrometeorological parameters and Energy Fluxes at an intertidal zone of a Tropical Coastal Ocean, Data Brief, 21, 13–17, https://doi.org/10.1016/j.dib.2018.09.108, 2018a.

Yusup, Y., Alkarkhi, A. F. M., Kayode, J. S., and Alqaraghuli, W. A. A.: Statistical modeling the effects of microclimate
635 variables on carbon dioxide flux at the tropical coastal ocean in the southern South China Sea, Dynamics of Atmospheres
  and Oceans, 84, 10–21, https://doi.org/10.1016/j.dynatmoce.2018.08.002, 2018b.

Yusup, Y., Ramli, N. K., Kayode, J. S., Yin, C. S., Hisham, S., Isa, H. M., and Ahmad, M. I.: Atmospheric carbon dioxide
  and electricity production due to lockdown, Sustainability (Switzerland), 12, 1–12, https://doi.org/10.3390/su12229397,
  2020.

640 Zhang, H. F., Chen, B. Z., van der Laan-Luijkx, I. T., Chen, J., Xu, G., Yan, J. W., Zhou, L. X., Fukuyama, Y., Tans, P. P.,
  and Peters, W.: Net terrestrial CO_2 exchange over China during 2001–2010 estimated with an ensemble data assimilation
  system for atmospheric CO2, J Geophys Res, 119, 3500–3515, https://doi.org/10.1002/2013JD021297, 2014.